



## Towards feasibility of photovoltaic road for urban traffic-solar energy estimation using street view image

Ziyu Liu<sup>a</sup>, Anqi Yang<sup>a</sup>, Mengyao Gao<sup>a</sup>, Hong Jiang<sup>a</sup>, Yuhao Kang<sup>a, b, c</sup>, Fan Zhang<sup>c</sup>, Teng Fei<sup>a, \*</sup>

<sup>a</sup> School of Resources and Environment Sciences, Wuhan University, Wuhan, Hubei, 430079, China

<sup>b</sup> Geospatial Data Science Lab, Department of Geography, University of Wisconsin-Madison, Madison, WI, 53706, USA

<sup>c</sup> Senseable City Lab, Massachusetts Institute of Technology, Cambridge, MA, 0213, USA

### ARTICLE INFO

#### Article history:

Received 7 January 2019

Received in revised form

19 April 2019

Accepted 20 April 2019

Available online 23 April 2019

#### Keywords:

Clean energy

Solar radiation

Photovoltaic road

Street view

### ABSTRACT

A sustainable city relies on renewable energy, which promotes the development of electric vehicles. To support electric vehicles, the concept of charging vehicles while driving has been put forward. Under such circumstances, constructing solar panels on urban roads is an innovative option with great benefits, and the accurate calculation of road photovoltaic power generation is a prerequisite. In this paper, we propose a novel framework for predicting and calculating the solar radiation and electric energy that can be collected from the roads. Google Street View images are collected to measure the sky obstruction of roads which is integrated with the solar radiation model to estimate the irradiation receiving capability. In addition to sky obstruction, we also take the impact of traffic conditions and weather situations into consideration in the calculation. Radiation maps at different times in a year are produced from our work to analyze the roads photovoltaic distribution. In order to test the feasibility of our framework, we take Boston as a case study. Results show that roads in Boston can generate abundant electricity for all future electric vehicles in the city. What's more, main roads through Boston exhibit better power generation potential, and the effect of the traffic condition is limited. Our calculation framework confirms that utilizing solar panels as road surfaces is a great supplement of city power with the unique ability to charge moving cars.

© 2019 Elsevier Ltd. All rights reserved.

### 1. Introduction

Since the concept of “sustainable city” has been put forward, new and renewable energy resources have gained increasing attention (Jacobson, 2009; Kenworthy, 2006). For the development and utilization of clean alternative energy, the electric vehicle industry has matured and prospered with technical progress (Zhao and Zhao, 2015). From the early 1990s, the world's major automobile group companies such as Ford, GM, etc. have invested a large amount of resources in the field of electric vehicles (Cao et al., 2004) to achieve zero emissions of cars. The driving range which is determined by the battery, however, is the main factor that hinders the diffusion and popularization of electric vehicles (Kessels et al., 2011). Compared to decades ago, the successful evolution of battery materials has extensively increased the driving range before

needing to stop the vehicle for charging. Currently, it is facing more challenges. Another alternative is to charge moving vehicles “on-the-fly” based on technologies like contactless power transfer systems (Chopra and Bauer, 2013).

Although solar power is one of the cleanest energies for a city (Kamat, 2007), large-scale solar power generation, like building traditional power plants (solar farms), has the following special requirements: being built in open areas with sufficient sunshine, and occupying a vast expand of area in suburb, which inevitably results in long-distant electricity transmission and a waste of space. On the contrary, urban road surfaces, which occupy a large part of public areas (Northmore, 2014) in a city, may also get adequate sunshine. Therefore, in terms of the energy needs for intra-city transportation, laying photovoltaic power generation materials such as special solar panels on the roads (Northmore and Tighe, 2012) has greater advantages of saving space and transferring power compared with the traditional solar farm system. Some countries and regions in the world have already made efforts to

\* Corresponding author.

E-mail address: [feiteng@whu.edu.cn](mailto:feiteng@whu.edu.cn) (T. Fei).

**Table 1**  
Current demonstration projects about photovoltaic roads.

City	Year	Details of solar road	Production	Cost
Amsterdam, Netherlands (Contributor, 2016; Rooij, 2017)	2014	a 70-m bike path was replaced by solar panels	It generated 3000 kWh in just half a year after its construction	\$3.7 million totally
Normandy, France (Dockrill, 2016)	2016	A one-kilometer-long solar highway.	it is projected to produce 280 MWh of energy annually, with an estimated electrical output of 767 kWh per day.	\$1850, per square meter
Jinan, China (Cooke, 2017; Liang, 2017)	2017	a 1 km stretch of solar highway	It can generate one million kWh of clean power every year, enough to meet the daily needs of roughly 800 households.	\$458, per square meter

pave photovoltaic roads. Several projects are shown in Table 1.

Although road photovoltaic generation sounds feasible, exposed photovoltaic panels would be subjected to dust, heavy weight, weathering, pollution, and even acidic rain etc. Many researchers have devoted in the advancement of solar panel material in order to promote it to practical application of road (Gilpin, 2014; Rahman et al., 2018; Roadways, 2018), which also requires high cost (Lee, 2016; Macdonald, 2015). Such limitation implies the accurate calculation of road photovoltaic power generation is a prerequisite, while there is no existing work related to the assessment of road photovoltaic capacity yet. Additionally, the orientation, the vegetation and the canyon of streets could obstruct the incoming solar radiation, which consequently would reduce the productivity of road photovoltaic generation (Northmore and Tighe, 2012). Street canyon here is a canyon-like environment where the street is flanked by buildings on both sides. As a result, the high-cost photovoltaic roads construction entails rigorous selection as well as planning since replacing all the city roads with solar panels is actually extravagant, and could hinder the economy during construction if the efficiency of the panels does not meet energy demands. Therefore, the availability of road solar radiation is an essential issue for planning the installations of solar roads.

The research of solar radiation has attracted a lot of attention for a long time due to its applications in many fields (Ahmad and Tiwari, 2011; Chegaar and Chibani, 2000; Ya'u et al., 2018). Researchers in different fields proposed several solar radiation calculation methods and gained good results under diverse circumstances, like climate studies (Chou, 1992), crop growth (Bojanowski et al., 2013), environmental thermal comfort (Gennusa et al., 2007), photovoltaic potential assessment (Súri and Hofierka, 2010), terrain, etc. (Rich, 2000). As streets are the main space for urban travels, many scholars studied solar radiation in street canyons as well (Ali-Toudert and Mayer, 2006; Alnaser et al., 2017; Mk, 2010). This derives a term called "Street View Factor" (SVF) which represents the ratio of radiation received (or transmitted) from the sky plane to that emitted (or received) from the entire hemispherical radiation environment (Chen et al., 2012; Watson and Johnson, 2010). The focus on SVF promotes the significance of horizon obstruction in solar radiation.

Since SVF plays an important role in assessing street solar availability, many methods are proposed to calculate the street solar radiation based on SVF. These methods can be mainly divided into three categories (Table 2).

Considering these disadvantages mentioned in Table 2, Street View images provide a good alternative because they have an upward view and can access uniform, real street images containing trees, buildings along with all other elements that influence SVF. As a high resolution online geospatial data source (Rousselet et al., 2013), Google Street View (GSV) provides 360° panoramic street-level images which are road scenes with surrounding trees and buildings. These images constitute a huge street view database covering an extensive area with free access (Anguelov et al., 2010), which contributes to the advantages of using GSV to measure SVF automatically and in batches. Since GSV has been launched in the public, related work has emerged in various research orientations. Notably, in environmental reconstruction, Torii et al. (2009) used GSV to construct 3-D city models, Rundle et al. (2011) used GSV to assess the neighborhood environment, and Zhang et al (2018) used GSV to study human perceptions in urban scenes. Another GSV topic is to identify visual features in street view images for analysis. For example, Long and Liu (2017) evaluated the street greenery from GSV, while Zamir et al. (2012) utilized the textual information to identify the commercial entities in street view imagery. In addition, sky extraction of street view images enables the measurement of SVF and solar radiation. Carrasco-Hernandez et al. (2015) proves that the reconstruction of urban geometries from GSV has potential use for scientific purposes like SVF calculation.

To assess the solar radiation received by the street, traffic conditions are indispensable factors to be considered as vehicles will occupy the road surface and block the solar radiation from collection. Therefore, we need to calculate the impact of urban traffic on the collection of solar energy. Furthermore, it is necessary to understand the relationship between the traffic speed and traffic density for accurate results. Early in 1935, Greenshields (1935) developed a new method which uses traffic speed and traffic density to measure traffic flows. Since then, more studies carried out similar methods to discover more models of road traffic, like *cellular automata* (CA) traffic model (Hong-Wu, 2006), and flow-density relation (Kim and Keller, 2008). Since the real traffic condition is too complex to describe precisely, we take the traffic big data plus Greenshield's model and build the urban traffic model as realistically as possible. Effectively, we simulate the urban traffic conditions for precise and realistic analysis of road solar radiation.

In this study, we propose a novel framework to predict the electric energy based on road photovoltaic generation. We combine the GSV image data, the improved solar radiation model, and the

**Table 2**  
Three categories of methods to calculate solar radiation with SVF.

Method	Advantages	Disadvantages
<i>Geometrical Methods</i> (Watson and Johnson, 2010)	It uses measured parameters of street buildings to measure the street geometry accurately.	It ignores the important sky-shading factors such as street trees around the buildings.
<i>3D Urban Model</i> (Hofierka and Kaňuk, 2009; Unger, 2009).	3D urban models with building information are widely applied in SVF.	There's a gap between the actual situation of the street and the model like trees etc. It also has extremely high costs and long update intervals.
<i>Digital Images</i> (Cristina S. Polo López et al., 2016; Matzarakis et al., 2010)	There are great sources of street information to describe street geometry and SVF elaborately.	Such manual image collection requirement and processing are inconvenient for batch processing automatically.

street geometry measurement, to calculate the solar radiation obtained by road accurately. Then, the traffic flow model is implemented in the research while the time period in which the road can be irradiated is also calculated. Finally, we apply the methods to Boston by computing the photovoltaic generation capacity in the urban street to test the feasibility of our framework. Our results can provide an advocacy and guiding for the paving of the photovoltaic road in cities like Boston to address the increasing popularity of electronic vehicles. Since our framework is universal, the method to assess the capacity of photovoltaic roads not only apply to Boston but any other cities with street view.

## 2. Methodology

This section introduces the method of calculating the solar irradiance received by urban streets in detail. It is divided into four parts. The first procedure is data collection. And then is the data processing part. The third step is to utilize the solar radiation model with processed GSV images to calculate the net solar radiation received by the empty road. The last part is to utilize the traffic flow model to simulate the impact of roads' traffic conditions on the solar radiation received. Our research also explores the potential applications based on our framework. Fig. 1 is the conceptual diagram of our method.

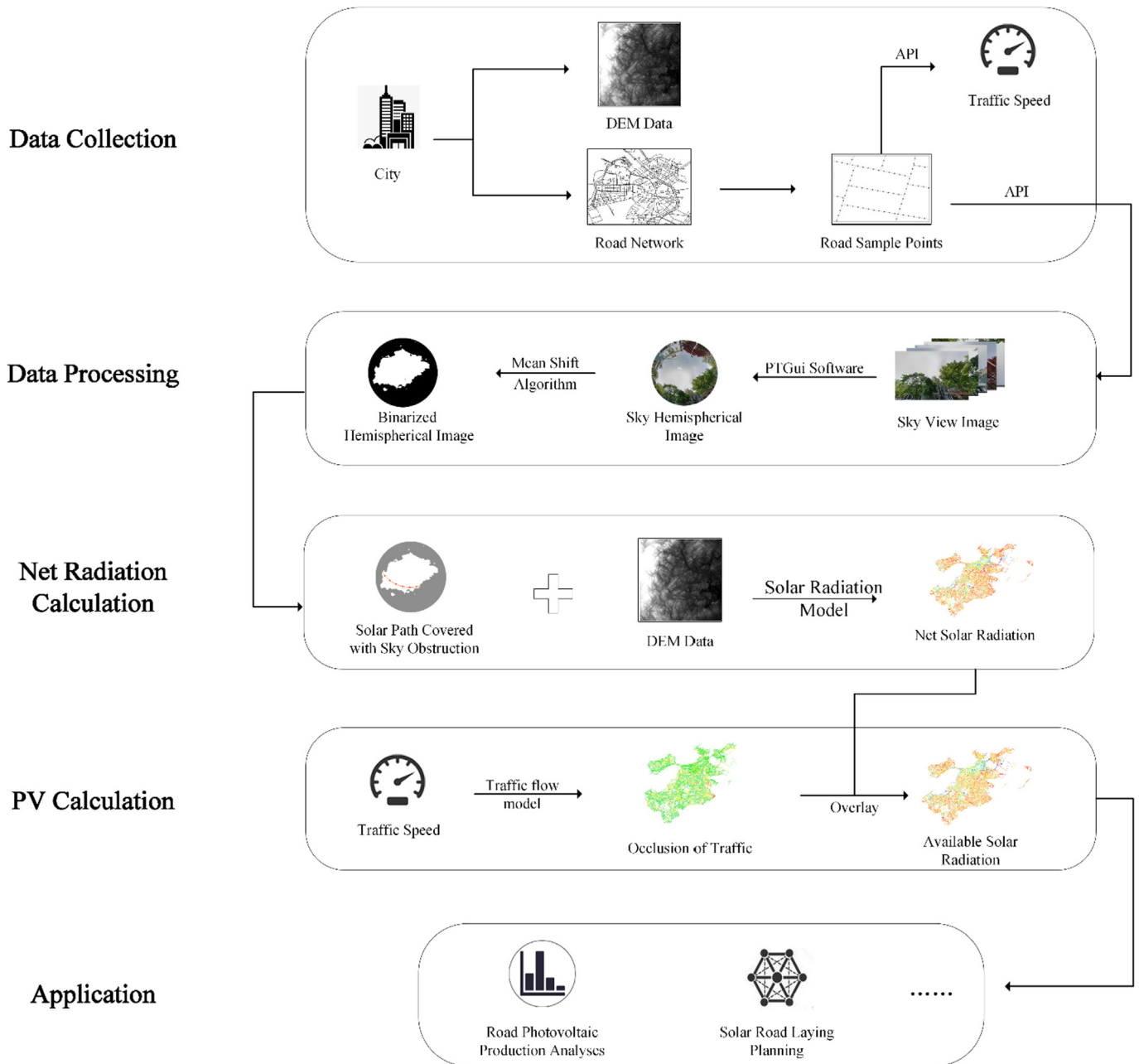
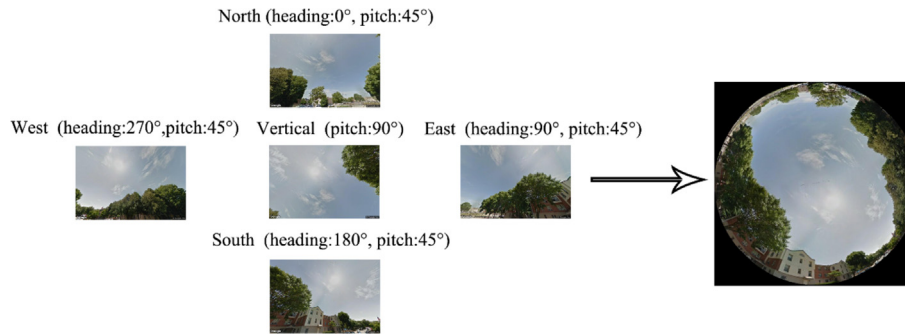


Fig. 1. The flow chart of the method.



**Fig. 2.** GSV images in different directions (left) and hemispherical panorama image (right). Heading is the horizontal angle relative to the north of the camera while pitch is the vertical angle relative to the horizontal plane of the camera.

## 2.1. Data collection and processing

The description of street geometry in the vertical direction is essential to road solar radiation calculation in the street canyon. This means an upward-looking 360-degree panorama is required. GSV provides a suitable data source to reconstruct the street geometry at any point on streets, allowing us to build sky hemispherical images in which the portion of clear view of the sky from that point can be calculated. The sky extraction process has three steps: the acquisition of GSV images, the generation of sky hemisphere pictures, and the binarization of the sky.

### 2.1.1. The acquisition of GSV images

Google Maps Platform provides an open API<sup>1</sup> for users to acquire GSV photos. Users can send requests with coordinates and other parameters of the target position to get a static street view. We take the road points with coordinates data extracted from the city roads as input to acquire the real street images. In order to get the hemispherical image of the sky, the following five 600 × 400-pixel images with a 120-degree-view in different directions are required: four images with heading of East, West, South and North, and one with an upward view (Fig. 2).

### 2.1.2. Sky hemispherical images

We adopt PTGui software to stitch five GSV pictures together of one point mentioned above, and a 644 × 644-pixel hemisphere sky fisheye image is constructed (Fig. 2). Such an image processing tool stitches pictures together by converting control points that are similar in the contiguous two pictures to reference points to realize image registration and hemispherical panoramas generation, accurately and efficiently. During the image process, we utilize a hemispherical equidistant projection to project the image in the vertical direction to acquire a 360-degree image. The equidistant projection with the attribution of the undistorted distance from any pixel to the center point of the image can help simplify the further calculation.

### 2.1.3. Sky element extraction through binarization

As hemispherical images represent the upward scene from the ground, sky sections are the origination of solar light to the points in these images as well as the source of solar radiation within street canyons. To calculate the angles of obstruction range, extracting the sky from hemispherical images is a prerequisite. Intuitively, several objects like the sky, buildings, and trees in the street view images have distinct boundaries, which means pixels show the same

objects. In addition, they have similar visual characteristics and are aggregated.

We first used the mean shift algorithm to detect such objects in the image (D. Comaniciu, 2002). The mean shift clustering algorithm is a non-parametric feature-space analysis technique for locating the maxima of a density function, a so-called mode-seeking algorithm which is capable of handling arbitrary feature spaces and can be applied to cluster analysis in computer vision and image processing (Cheng, 1995). And it has been used in existing related work to extract sky from street view images, which shows the efficacy of such algorithm (Li and Ratti, 2018; Sirmacek, 2011). Through the algorithm, nearby pixels with similar spectral information are aggregated into the same objects. Generally, sky is mostly blue and as the light source is the brightest section of the images, the sky part is brighter than the non-sky part in the blue channel of the image. Considering the facts mentioned above as well as the parameters recommended by previous research (Li and Ratti, 2018), we used a modified brightness to extract sky pixels, which reduces the weight of red band and increases the weight of blue band. The value is calculated as follow:

$$\text{Brightness} = (0.5 \times R + G + 1.5 \times B) / 3 \quad (1)$$

Where R, G and B indicate the pixel values in red, green and blue channel respectively. Pixels with higher *brightness* have a higher possibility to belong to the sky part. To get the optimum threshold which provides the best value to distinguish the sky pixels and non-sky pixels, we apply Otsu's method (Otsu, 1979). The method aims at finding a global threshold automatically at the balance of maximum between-class variance and minimum within-class variance. As a result, all but the sky pixels are considered obstruction pixels which are processed as a binarized picture later. Each raster cell in the binarized images specifies a value that indicates whether the sky direction is visible (white pixel) or occluded (black pixel).

## 2.2. Solar radiation model

The calculation of street solar radiation evolved from spatial insolation models (Flint and Childs, 1987; Rich, 1990; Swift, 1976). Solar radiation emits through the atmosphere from the path of sun. The energy radiated to the surface modified by topography and other surface features are mainly divided into three components: direct, scattered and reflected insolation. Direct light is generally the most important source of radiation. The diffuse is the second, while the reflection can be neglected with a limited impact. The calculation model for global solar radiation is:

<sup>1</sup> <https://developers.google.com/maps/documentation/streetview/intro>.

$$Global = Dir + Dif \tag{2}$$

where *Global* represents global radiation; *Dir* is the component of direct radiation; *Dif* is the component of diffuse radiation.

2.2.1. Sky viewshed calculation

The actual insolation intercepted by the surface is greatly influenced by the obstruction of sky. In particular, it is the part that blocks the sun track. Therefore, calculating the range of the sky viewshed is the core algorithm of this section. In the hemispherical viewshed algorithm developed by Fu and Rich (2002), the range of the sky viewshed is derived from DEM data. We replace it with a binarized GSV image generated from part 1. The binarized sky hemispherical images are used directly as the 2-D raster data of the equirectangular projection, so the zenith angle  $z$  (angle formed by the direction of the vertical direction) and the azimuth angle  $\alpha$  (angle formed by the north direction) of the visible sky in hemisphere can be inversely calculated according to the pixel position in 2-D coordinates of the image as Fig. 3. Combined with the position of sun and the deviation of the sky (represented by Sunmap and Skymap respectively), we calculate the direct, diffuse and global insolation of each interested position.

In Fig. 3, gray pixels represent the non-sky area, while white represent the sky. The hemisphere radius ( $R$ ) is half of the image size: 322 pixels. The equirectangular projection transformation formula is used to convert the raster pixel coordinates into a 3-D hemispherical coordinates.

2.2.2. Sunmap and Skymap calculation

Sunmap (Fig. 4) is a raster representation of the sun tracks over a certain area which is determined by latitude and varies through times and seasons, so it's used for the calculation of direct radiation. Particularly, Sunmap consists of discrete tiny sectors shown in Fig. 4

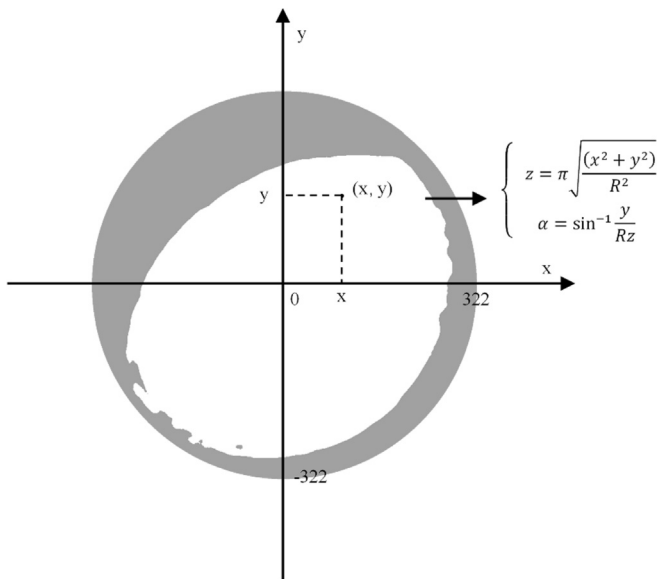


Fig. 3. Image of convert plane coordination system to hemispherical coordination system. The point in the plane coordination system has coordinates (x, y) which can calculate the zenith angle ( $z$ ) and azimuth angle ( $\alpha$ ) in the hemispherical coordination system using the equations in this image.  $R$  is the hemisphere radius (322 pixels) here.

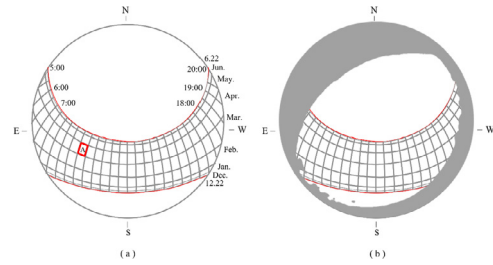


Fig. 4. (a) Sunmap for Winter Solstice to Summer Solstice; (b) Sunmap with obstruction. Such Sunmap is from Winter Solstice to Summer Solstice for 42.3°N latitude using 0.5 h intervals through a day and month intervals through a year.

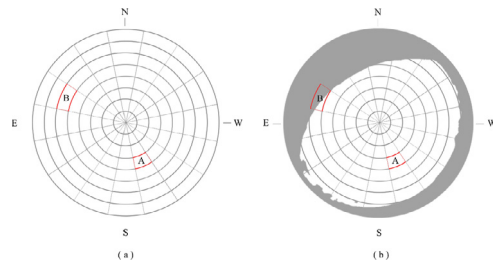


Fig. 5. (a) Skymap with sky sectors defined by 16 zenith divisions and 8 azimuth divisions; (b) Skymap covered by obstruction.

a. These sectors are defined by the position of the sun at a given day (hours) and year (days or months) corresponding to the horizontal and vertical intervals respectively. The two red lines in Fig. 4 are the sun paths in June 22nd and December 22nd which are the northern and southern boundaries of the positions of the sun in the sky during a whole year. Additionally, the red marked sector (A) is the range of the sun position between 9:30 am and 10:00 am in April. Besides, locations in the same area have the same Sunmap as the area is relatively small.

Skymap (Fig. 5) is used to calculate the diffuse radiation. The diffuse radiation from each sky direction is the result of the dispersing light from atmospheric components such as clouds and particles. To calculate, Skymap is divided into a series of sectors as a hemispherical view of the entire sky. These tiny sky sectors in Fig. 5 are defined by 8 zenith segments and 16 azimuth segments. As shown in Fig. 5, red marked sectors (A) and (B) are two pieces of the discrete sky. Since their positions described by the zenith and azimuth angles of their sector centroids are different, the diffuse radiation passing through each part is different. What's more, the obstruction covers most of Sector (B), while having no influence on Sector (A), which increases the gap between these two sectors. Follow the default number from the referred guidance (Rich, 2000), we set the sector numbers as Fig. 5.

We calculate the sun path over the study area by the solar model and plot it in a grid image with a fixed resolution and time intervals. The map resolution and projection are consistent with the binary image. Each sector in the Sunmap represents the position of the sun in each month with a time resolution of 0.5 h. On both Sunmap and Skymap, the solar track of the visible area is recorded, and the integral of direct and diffuse radiation at given time period are calculated.

## 2.2.3. Solar radiation calculation

flow which will be discussed later.  $G_z$  is the surface zenith angle

Nomenclature Explanation		Nomenclature Explanation	
$Global$	global radiation (Wh/m <sup>2</sup> )	$\alpha$	azimuth angle (degrees)
$Dir$	direct radiation (Wh/m <sup>2</sup> )	$z$	zenith angle (degrees)
$Dif$	Diffuse radiation (Wh/m <sup>2</sup> )	$\beta$	atmospheric transmittance (dimensionless)
$S_{Const}$	solar constant (WM <sup>-2</sup> )	$m(z)$	Relative optical length (dimensionless)
$SunDur$	Sun duration (hours)	$Ele\upsilon$	Elevation (m)
$SunGap$	the sky proportion (dimensionless)	$G_z$	surface zenith angle (degrees)
$AngIn$	the angle of incidence (degrees)	$G_\alpha$	surface azimuth angle (degrees)
$R_{traffic}$	ratio of the traffic coverage on road (dimensionless)	$P_{dif}$	proportion of global normal radiation flux (dimensionless)
$R_{glb}$	the angle of incidence (degrees)	$Dur$	Sun Duration (hours)
$Weight$	ratio of diffuse radiation (dimensionless)	$z_1, z_2$	the zenith angles of the sky sector bounding (degrees)
$Pow_{annual}$	the annual photovoltaic power generation (Wh)	$Area_{tot}$	the total area of solar panels (m <sup>2</sup> )
$Pho_e$	the photoelectric conversion efficiency (dimensionless)	$K$	traffic density (Vehicles/km)
$N$	Numbers of vehicles (Vehicles)	$L$	Length of vehicle (km)
$V$	speeds of vehicle (km/h)	$K_j$	Blocking Density (Vehicles/km)
$V_f$	the theoretical maximum speed the same with smooth velocity (km/h)	$a, b$	The unknown coefficient of linear density-velocity model (dimensionless)

Then we develop a simple transmission model for solar radiation calculation (Pearcy, 1989; Rich, 1989, 1990). As mentioned above, we calculate direct radiation ( $Dir$ ) measured by Sunmap and the diffuse radiation ( $Dif$ ) measured by Skymap, which are both the sum of visible sectors ( $Dir_{z,\alpha}, Dif_{z,\alpha}$ ) in the map:

$$Dir = \sum Dir_{z,\alpha} \quad (3)$$

$$Dif = \sum Dif_{z,\alpha} \quad (4)$$

where  $z$  is the zenith angle of specified sector;  $\alpha$  is the azimuth angle of the sector.

In the Sunmap, the calculation of direct radiation from each sector ( $Dir_{z,\alpha}$ ) with a centroid at zenith angle ( $z$ ) and azimuth angle ( $\alpha$ ) is as follows:

$$Dir_{z,\alpha} = S_{Const} * \beta^{m(z)} * SunDur_{z,\alpha} * SunGap_{z,\alpha} * \cos(AngIn_{z,\alpha}) * (1 - R_{traffic}) \quad (5)$$

$$m(z) = \exp(-0.000118 * Ele\upsilon - 1.638 * 10^{-9} * Ele\upsilon^2) / \cos(z) \quad (6)$$

$$AngIn_{z,\alpha} = \cos^{-1}(\cos(z) * \cos(G_z) + \sin(z) * \sin(G_z) * \cos(\alpha - G_\alpha)) \quad (7)$$

where  $S_{Const}$  is the solar constant referred as the solar flux outside the atmosphere at the mean earth-sun distance. Here we adopt the World Radiation Center (WRC) solar constant as 1367 WM<sup>-2</sup>,  $\beta$  is the atmospheric transmittance, that is, the fraction of radiation that passes through the atmosphere (averaged over all wavelengths). Values range from 0 (no transmission) to 1 (all transmission), and 0.5 is for a generally clear sky.  $m(z)$  is the relative optical path length accounted for the zenith angle of solar position  $z$  and elevation ( $Ele\upsilon$ ) above sea level in meters (Equation (6)),  $SunDur_{z,\alpha}$  is the time intervals of configuration,  $SunGap_{z,\alpha}$  is the sky proportion of each Sunmap sector,  $AngIn_{z,\alpha}$  is the angle of incidence between the centroid of sectors and the normal axis of surface considering the influence of land surface on the radiation (Equation (7)),  $R_{traffic}$  is the ratio of the coverage on road resulted from traffic

referred as aspect of the surface,  $G_\alpha$  is the surface azimuth angle referred as slope of the surface.

In Skymap, we use the uniform diffuse model which assumes that incoming diffuse radiation is the same from all directions, to calculate diffuse radiation. For each sector's diffuse radiation ( $Dif_{z,\alpha}$ ), the calculation equations are as follows:

$$Dif_{z,\alpha} = R_{glb} * P_{dif} * Dur * SkyGap_{z,\alpha} * Weight_{z,\alpha} * \cos(AngIn_{z,\alpha}) * (1 - R_{traffic}) \quad (8)$$

$$R_{glb} = (S_{Const} \sum (\beta^{m(z)})) / (1 - P_{dif}) \quad (9)$$

$$Weight_{z,\alpha} = (\cos z_2 - \cos z_1) / Div_{azi} \quad (10)$$

where  $R_{glb}$  is the global normal radiation (Equation (9)),  $P_{dif}$  is the proportion of global normal radiation flux that is diffuse. The value ranges from 0 (clear sky) to 1 (cloudy sky) according to atmospheric conditions which can refer to the proportion of cloudy days to sunny days in a city.  $Dur$  is the time interval corresponding to the Sunmap.  $SkyGap_{z,\alpha}$  is the sky proportion of each Skymap sector,  $Weight_{z,\alpha}$  is the ratio of diffuse radiation in the given sky sector to all sectors (Equation (10)),  $Div_{azi}$  is the number of azimuth segments in Skymap.

The results of Equation (2) indicate the solar panels built on the roads can receive such amount of solar radiation. It still needs conversion to electricity by the following equation:

$$Pow_{annual} = Global_{annual} * Area_{tot} * Pho_e \quad (11)$$

where  $Pow_{annual}$  is the annual photovoltaic power generation,  $Global_{annual}$  is the annual global solar radiation,  $Area_{tot}$  is the total area of solar panels, and  $Pho_e$  is the photoelectric conversion efficiency.

$Area_{tot}$  is determined by road width and length. For a sample point, the length is the intervals between two adjacent points, while the width is related to road type. We measured each type of roads on Google Maps with the measuring tools provided to obtain the width data.

## 2.3. Traffic model

Although we calculate the road net solar radiation, it is not

actually usable for roads that are always occupied by traffic which has negative impact on the ultimate availability of solar radiation. Especially when there's a traffic jam, the roads almost receive no illumination of the sun. Therefore, it is necessary to overlay the empty roads with the traffic conditions and obtain shielding proportion of the roads by the relationship between car speed and traffic density.

### 2.3.1. Acquisition of traffic flow data

TomTom<sup>2</sup> traffic online provides accurate traffic information, including the real-time traffic conditions, traffic jams and traffic accidents. We obtain the real-time observation speed of the nearest road around the given point from the free Traffic flow API interface.

We dilute the original road pointset into points separated by 100m as input, send requests to the API, and then record the road real-time speed at the time of request. The speed values of all road segments are obtained both on the workday and the weekend at an interval of 1 h from sunrise to sunset as representations of normal traffic conditions.

### 2.3.2. Traffic flow model

Traffic Flow Model (Greenshields et al., 1934) considers the relationship between traffic speed and traffic density which refers to the intensity of vehicles on a lane, that is, the number of vehicles on a lane per unit length at a certain moment. Assuming that the traffic flow is free, there are  $N$  vehicles continuously advancing on the road section with length  $L$  at the speeds of  $V$ , then the traffic density  $K$  (Vehicles/Km) on the  $L$  section is:

$$K = \frac{N}{L} \quad (12)$$

We use linear density-velocity model to calculate density under different road level and velocity condition:

$$V = a - bK \quad (13)$$

when  $K = 0$  (free flow condition),  $V$  can reach the theoretical maximum speed the same with smooth velocity  $V_f$ , which means  $a = V_f$ ; when density reaches the maximum value  $K = K_j$  equivalent to  $V = 0$ , which means  $b = \frac{V_f}{K_j}$ . Here Blocking Density  $K_j$  is the density when the traffic flow is dense that all vehicles can't move. Smooth Velocity  $V_f$  is the average velocity when traffic density is almost 0, all vehicles can travel smoothly. We have:

$$V = a - bK = V_f - \frac{V_f}{K_j}K = V_f \left( 1 - \frac{K}{K_j} \right) \quad (14)$$

$$R_{\text{traffic}} = 1 - K \quad (15)$$

where  $V_f$  is replaced by freeFlowSpeed,  $V$  is the currentSpeed,  $K_j$  is the number of 4.5-m-long vehicles on a 1-km-long unit length of lane,  $K$  is the target value, the current road traffic density required. Finally, we convert the traffic density into the current road occlusion area ratio ( $R_{\text{traffic}}$ ) mentioned in the solar radiation model.

## 3. Case study

### 3.1. Study area

To apply our method, we chose Boston as a case study. Boston (Fig. 6) is a famous city that leads the development of

science and culture with many famous universities. It is on the edge of the Atlantic Ocean with an average elevation of 4m. Additionally, the seasonal average cloud coverage percentage in Boston shows minor fluctuation. There is a sunny season (from the end of June to early November) and a cloudy season (the rest part of year) in Boston annually. In 2018, about 60% days in the sunny season are sunny while only 48% of the chance in cloudy season. (Fig. 7a).

The daytime of Boston varies widely throughout the year (Fig. 7b). In 2018, the shortest day is December 21st, with 9 h and 5 min of daylight; the longest day is June 21st, with 15 h and 17 min of daylight (Cedar Lake Ventures, 2018).

### 3.2. Detailed method

The datasets used in the research applied in Boston are comprised of the DEM data, Boston road data, Google Street View (GSV) pictures, and traffic flow data from TomTom.

We collect GDEMDEM 30m image<sup>3</sup> (Fig. 6 a) of Boston in order to get the surface condition which determines the solar radiation by slope and aspect.

The Boston road networks (Fig. 6b) are derived from OpenStreetMap. We remove roads which are not wide enough for vehicles, like park paths, and get sample points with coordinates at an interval of 15 m along roads.

Then we apply our methodology to acquire Boston GSV pictures by sample points coordinates. Then these photos are used to generate binary fish-eye images to show the sky obstruction.

We then calculate the solar radiation received by roads without traffic. First, we compute the Sunmap and Skymap of Boston with the configuration of Boston latitude (42.3°N) and 0.5 h intervals through a day and month intervals through a year. Second, we overlay these two maps with processed pictures respectively to calculate the sky proportion of Sunmap and Skymap. Finally, with the DEM data, we calculate the net solar radiation of each point according to the solar radiation model. Here, we take Boston weather condition into consideration and divide the whole year into two parts (a sunny season and a cloudy season) with two different  $P_{\text{dif}}$  mentioned in Equations (10) (11) to calculate accurately.

The traffic flow data of real-time traffic conditions is firstly obtained by TomTom Online Traffic API<sup>4</sup>. Then we convert the large dataset into the roads' percentage of usable area which can be overlaid on the road net solar radiation. For a more accurate measurement, we define two traffic modes: workday mode and weekend mode to calculate separately. Fig. 8 shows the detailed flow of the application to Boston of our framework.

## 4. Results

### 4.1. Sky extraction of hemispherical GSV images

Fig. 9 shows the processed images in Boston. Images on the left are original hemispherical GSV images. We can recognize that objects in the image are mainly trees, buildings and the sky. After binarization, we get pictures on the right which distinguish the sky pixel from others clearly of whatever the remaining part are such as trees, buildings, and other constructions. In Boston, 122,226 GSV hemispherical binarized images are obtained.

<sup>3</sup> <http://www.gscloud.cn/>.

<sup>4</sup> <https://api.tomtom.com/traffic/services/4/flowSegmentData/absolute/10/json?params>.

<sup>5</sup> <https://www.openstreetmap.org/>.

<sup>2</sup> <https://developer.tomtom.com/>.

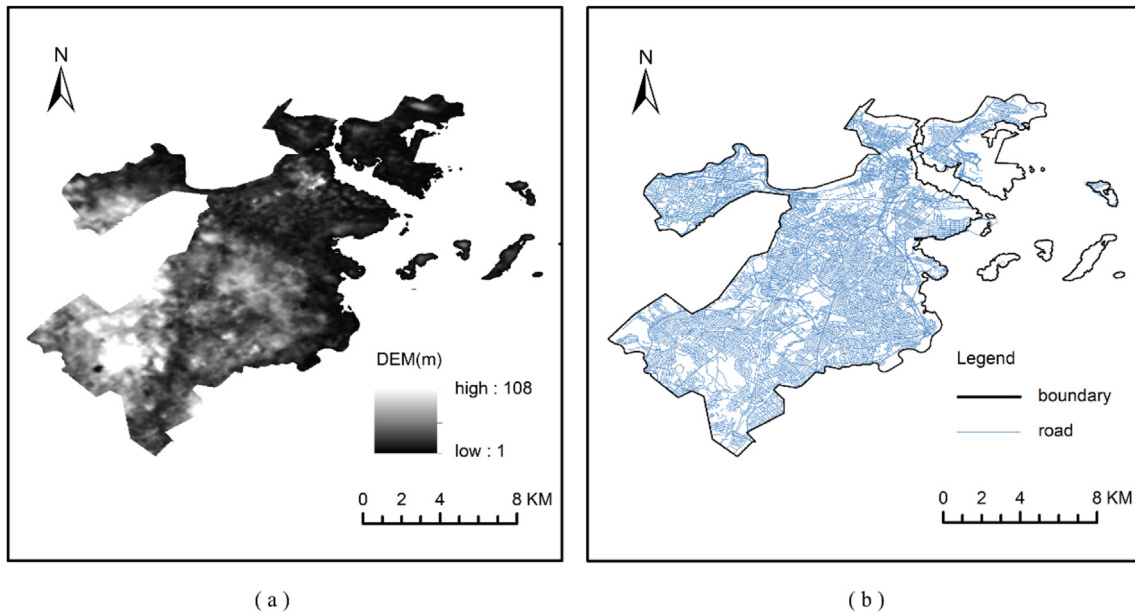


Fig. 6. Boston DEM image (a) and Boston road map (b).

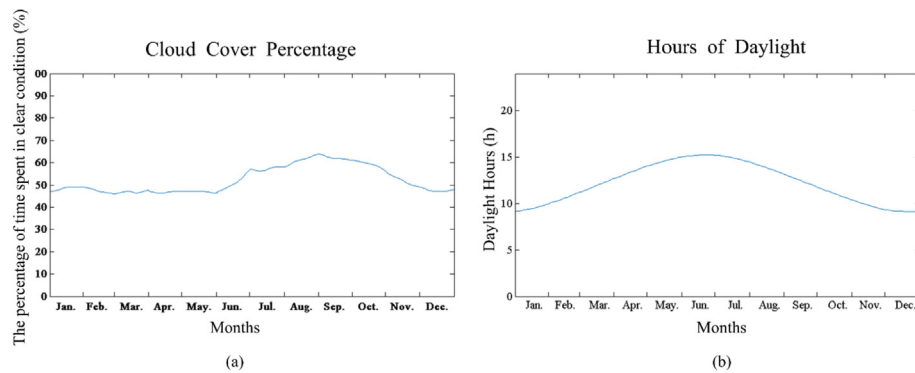


Fig. 7. 2018 Boston annual cloud cover (a) and Daylight hours (b).

#### 4.2. Calculation of solar radiation

The actual road solar radiation without traffic in Boston on the special position of sub-solar point in a year is calculated as follows: equinox (March 21st, September 21st) and solstice (June 22nd, December 22nd) separately. Since the sun track on autumn equinox is the same as the spring, we use spring equinox as a representation. Also, we calculate the whole year's radiation. As for the Boston sky clearness in a year, we assumed the  $P_{dif}$  to be 4.0 in sunny season and 5.2 in cloudy season according to its average cloud cover proportion (Fig. 7).

With regard to the special days of a year, the summer solstice has the year's longest daytime of about 15.5h known from the Sunmap whereas the winter solstice has the shortest of 9h. We set these days as a sunny day and interpolate grid maps (Fig. 10). The maximum value of solar radiation is 6391.01 WH/m<sup>2</sup> on the summer solstice and is only 871.08 WH/m<sup>2</sup> on winter solstice while it's 3499.12 WH/m<sup>2</sup> on spring equinox at a moderate level.

Spatially, the radiation distributions of the three days (Fig. 10 b, d, f) are basically consistent with the sunshine duration distributions (Fig. 10 a, c, e) and are similar to each other. The radiation received in downtown Boston (Northeast by center) is much lower than the rural area and the eastern and northeastern coastal part of

the area has higher solar radiation remarkably compared with the west corresponding to the sun duration distributions. Table 3 shows the difference among different dates plus the results of the whole year.

#### 4.3. Traffic condition in different modes

We plot the percentage of usable road area maps calculated from the current traffic flow speed both in workday mode and weekend mode (Fig. 11, Fig. 12). The study time of a day is from 5am to 8pm which covers the maximum span of Boston's daylight hours. We then apply the real time traffic speed at each hour for calculation.

Comparing these two modes, morning peak and evening peak are in workdays while the traffic is busy at 8am and from 12am to 6 pm at the weekend. Additionally, there exist roads occupied with vehicles during noon indicating that the road radiation is influenced negatively.

We take the day of June 22nd as an example to illustrate the influence on road solar radiation in different traffic modes. As the pictures show (Fig. 13), the maximum values are the same and the minimum values differ by only 0.002 Wh/m<sup>2</sup> between these two modes, the distributions are distinguished between the outskirts of

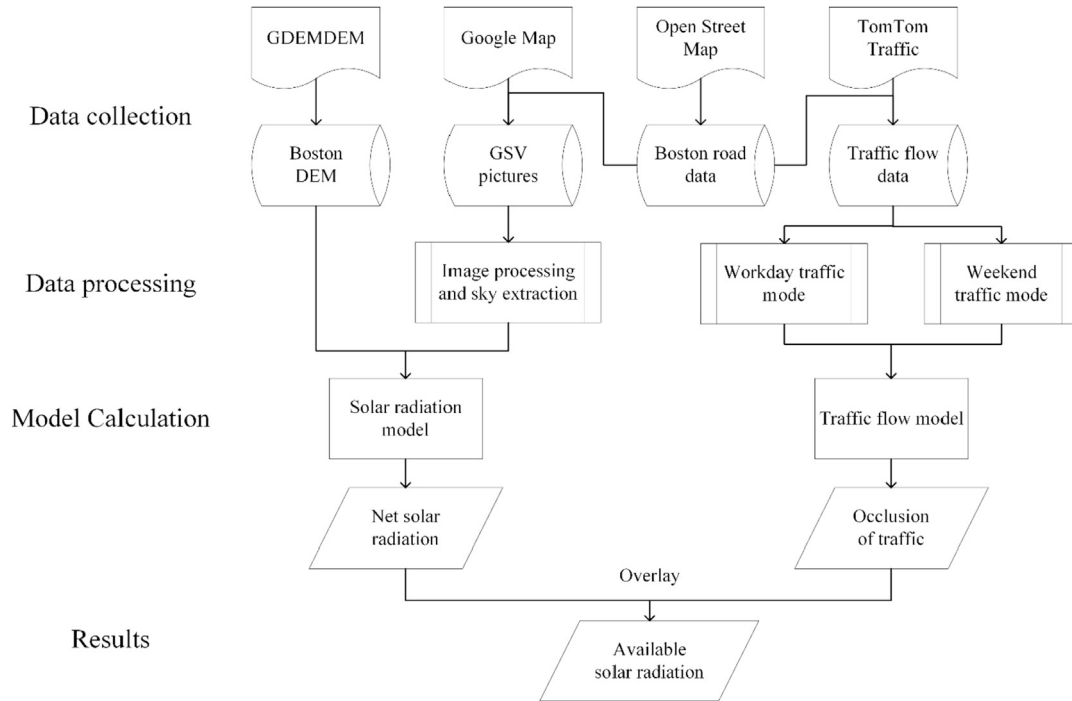


Fig. 8. The Flow Chart of Framework applied to Boston.

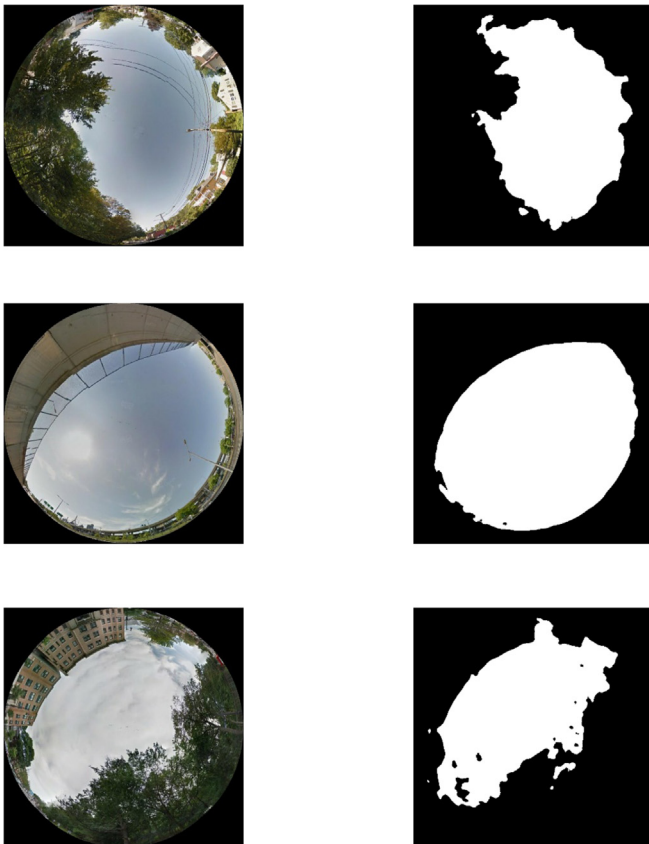


Fig. 9. Results of Hemispherical Panoramic image Binarization in different urban scenes.

downtown area with a higher radiation in weekend mode (Fig. 13 b, Fig. 13c). We use the weight of workdays and weekends in a week to calculate the conclusive influence of traffic on the radiation as a representation of typical traffic mode on that day. Compared with the road radiation in typical traffic mode (Fig. 13 d), the original solar radiation (Fig. 13a), only considering the street geometry obstruction, differentiates more on the main road radiation through Boston.

We calculate the radiation received in different times during a year (Table 4), the mean radiation with traffic is clearly less than that without traffic, and mean radiation in weekend mode is less than that in workday mode.

#### 4.4. Photovoltaic generation at street scale

Then we take the same street as an integral unit, rather than considering each point in the street, to analyze the distribution of the solar radiation and the actual photovoltaic generation in each road. As the photovoltaic closely relates to the road area, road width is a quite an important parameter. We measured the width of each road type shown in Table 5.

We assume that each point represents a road segment with solar panels whose length is 15-m-long (the interval of sample points). The width depends on the road type to receive solar radiation, and the photovoltaic conversion rate is 17% (ITRPV, 2018). We calculate each road photovoltaic generation in typical traffic modes and plot its distribution maps (Fig. 14).

Roughly, the pattern is inconsistent with the net solar radiation distribution in point scale as roads in the east are more efficient in photovoltaic generation. What's more, several main roads on the eastern and northwestern part obviously possess stronger power generation capacity. The values of the total and average road photovoltaic generation in typical traffic mode are shown in Table 6.

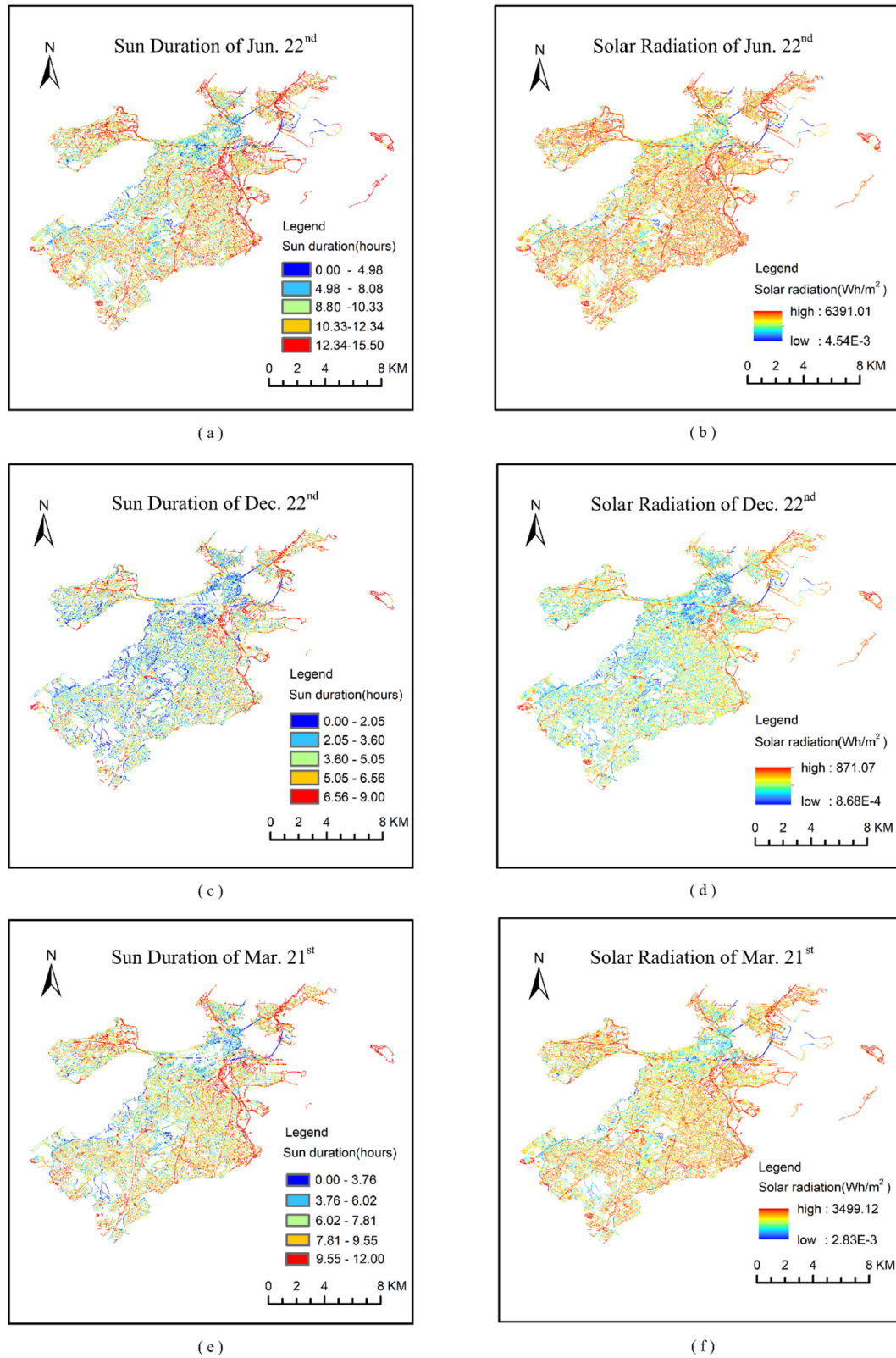


**Fig. 10.** The spatial distribution (point scale) of sun duration on June 22nd (a), Dec. 22nd (c) and Mar. 21st (e); The spatial distribution (point scale) of solar radiation on Jun. 22nd (b), Dec. 22nd (d) and Mar. 21st (f).



Fig. 11. Boston traffic condition on workday from 5 a.m. to 8 p.m.

4.5. Productivity efficiency at neighborhood scale

Since different neighborhoods have different road network structures, building styles and traffic conditions, which all influence the solar radiation, we calculate productivity efficiency of each neighborhood which is represented by the ratio of road photovoltaic output value to the neighborhood area and sort them (Fig. 15). Obviously, Downtown with busy traffic and lower solar radiation has a low productivity efficiency although it has a dense road network. Roads in West Roxbury, Hyde Park and East Boston receiving relative higher solar radiation yet have a low efficiency because of their sparse road network and vast area. Neighborhoods

like Allston, West End (the residential community), Charlestown, South Boston Waterfront (the Seaport District), all have light traffic and present a high productivity efficiency.

5. Discussion

This paper proposes a universal framework to calculate the usable solar radiation in a street environment based on the solar radiation model, street geometry, and traffic flow model. We take Boston as an example to valid the feasibility of the framework. The framework is completely independent and can be applied as long as the road network of the study city is covered by street view.



Fig. 12. Boston traffic condition at the weekend from 5 a.m. to 8 p.m.

Results show the immense potential of road power generation. We compute the total solar radiation and got  $1.304 \times 10^{10}$  kWh. Considering the solar irradiance-to-electricity conversion efficiency (17%), annual photovoltaic energy generated by roads in Boston is about  $2.216 \times 10^9$  kWh. Such much electricity can power 763.1 thousand electric vehicles under the assumption that each electric vehicle consumes 22 kWh electricity on average per hundred kilometer in downtown area (Energy, 2018), and each household car would run 1100 km a month on average. The number of household vehicles in Boston is about 272.6 thousand known from the Massachusetts Vehicle Census (MAPC, 2018). The results of a city's road power capacity are impressive, as the conversion

efficiency will be improved in the future, which contributes to the prospective improvement of the road photovoltaic capacity to power electric vehicles.

In order to decrease the impact of regional differences on research results and increase the persuasiveness of our results, we calculate each neighborhood's feasibility of road solar energy to supply their electric vehicles. In Fig. 16, the Supply-Demand ratio is the ratio of the total electricity demand for the vehicles (Lima et al., 2011) in each neighborhood to their road photovoltaic productivity. Clearly, except Back Bay which has few roads and more footway, the road electricity production of other any neighborhoods satisfy their own demand including both downtown and rural areas.

**Table 3**  
Comparison of road solar radiation without traffic at different times of the year.

Date/Period	Daytime (hours)	Road Solar Radiation Without traffic (Wh/m <sup>2</sup> )		
		max	mean	min
3.21	12.0	3499.12	2256.73	0.0028
6.22	15.5	6391.01	4604.90	0.0045
12.22	9.0	871.08	391.50	0.0009
<b>A Year</b>	8.5–15.5	1584489.69	1045436.38	0.4898

Many different types of regions all achieve a positive result, implying that the option of applying road photovoltaic system is not just a beneficial case for a specific city, since different neighborhoods have different characters which all influence the roads photovoltaic generation through the building, traffic, road greening

and so on. However, latitude is a significant factor that influences the receiving of solar radiation which is closely related to the location of the city. Although, Boston is a relatively high latitude city with abundant solar energy, the universality of this method also needs future research. In short, our framework provides a practical methodology for the accurate estimation of road solar power potential.

Considering the cost of solar road is too expensive currently, the minimum is up to \$458 per square meter (Cooke, 2017), what if the most efficient roads are selected to lay solar panels which have the maximum energy production per square meter? According to our calculation with the methods we presented, the roads that make up 32.4% of Boston’s total road area presented in Fig. 17 satisfy the current electricity demand for Boston domestic electric vehicles. Since these roads are about 4.3 million square meters, the cost of about 2 billion is quite unbearable now. However, while in the

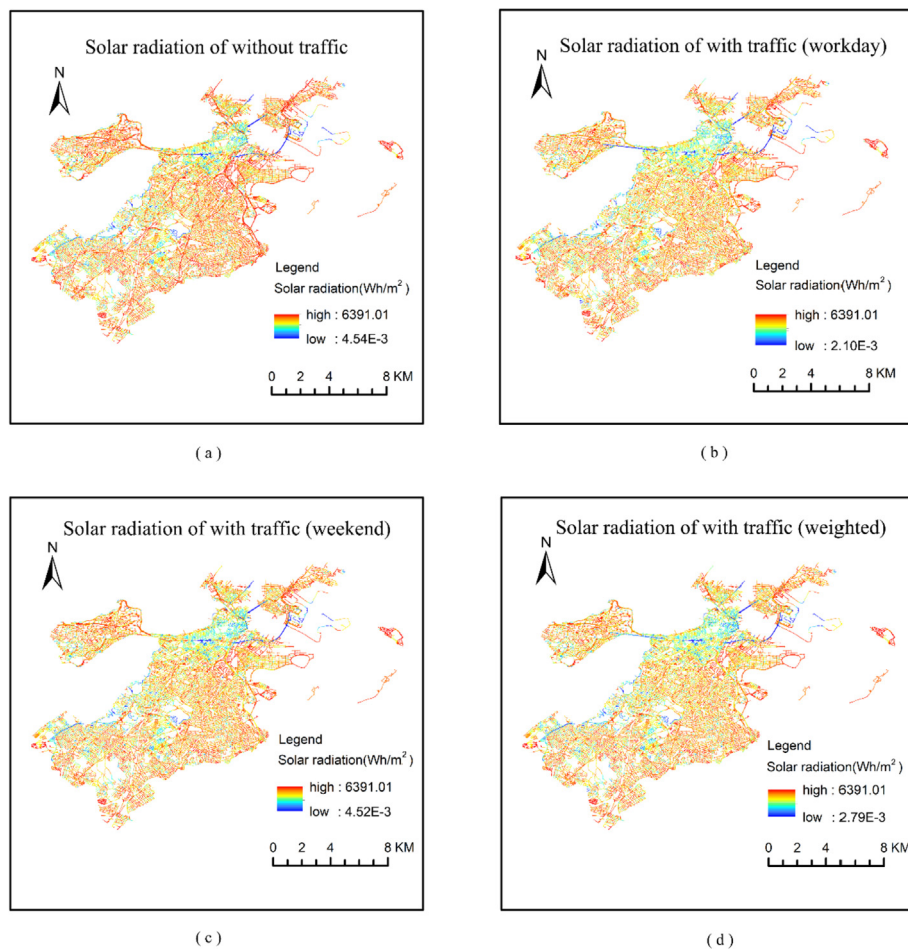


**Fig. 13.** Road radiation of Jun. 22nd without traffic (a), in workday traffic mode(b), in weekend traffic mode (c), and in typical traffic mode (d).

**Table 4**  
Mean Radiation under different traffic condition.

Date/Period	Mean Radiation without traffic (Wh/m <sup>2</sup> )	Mean Radiation With traffic (Wh/m <sup>2</sup> )		
		workday	weekend	Weighted <sup>a</sup>
3.21	2256.73	2117.49	2171.78	2133.00
6.22	4604.90	4316.96	4420.35	4346.50
12.22	391.50	367.11	378.22	370.28
<b>A Year</b>	1045436.38	986984.57	1007188.37	992757.084

<sup>a</sup> Weighted refers to typical traffic mode weighted according to the results of workdays and weekends. (typical=(5\*workday+2\*weekend)/7).

**Table 5**  
Road Width corresponding to Road Types.

Road Type <sup>a</sup>	motorway	trunk	primary	secondary	tertiary	unclassified	residential	service
Road Width (m)	13.5	9.3	9.7	9.8	9.2	6.6	5.5	6.7

<sup>a</sup> Road types are collected from OpenStreetMap.<sup>5</sup>

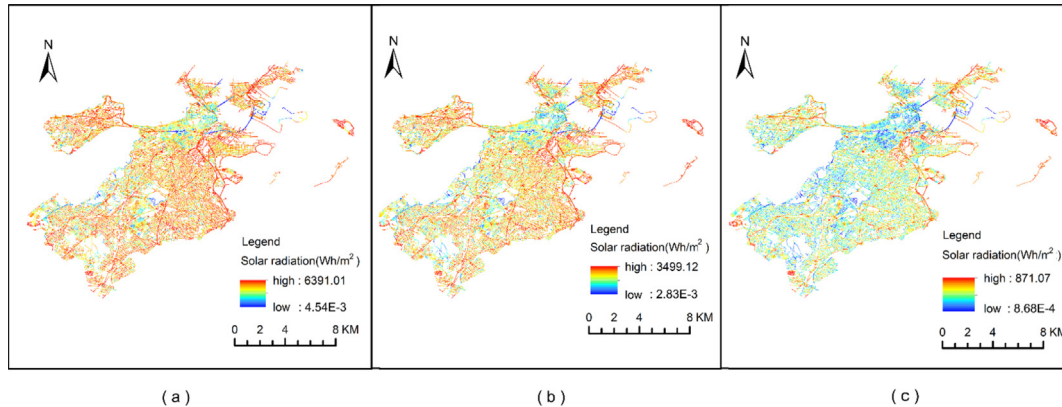


**Fig. 14.** The spatial distribution of solar radiation in street scale on June 22nd (a), Dec 22nd (b), Mar 21st (c).

**Table 6**  
Road photovoltaic power generation.

Date/Period	Average Road Photovoltaic Generation (Wh)	Total Ideal Road Photovoltaic Generation <sup>a</sup> (Wh)	Total Road Photovoltaic Generation (kWh)
3.21	36149.26	2.45E+7	4.77E+6
6.22	73599.70	5.70E+7	9.69E+6
12.22	6388.67	5.92E+6	8.38E+5
A Year	15507732.5	1.304E+10	2.216E+9

<sup>a</sup> Total Ideal Road Photovoltaic Generation is the result assuming 100% photoelectric conversion efficiency.

future the price reduced to similar to ordinary solar panels which is about \$124 per square meter (Austin, 2018), the idea of a photovoltaic road will pay big dividends.

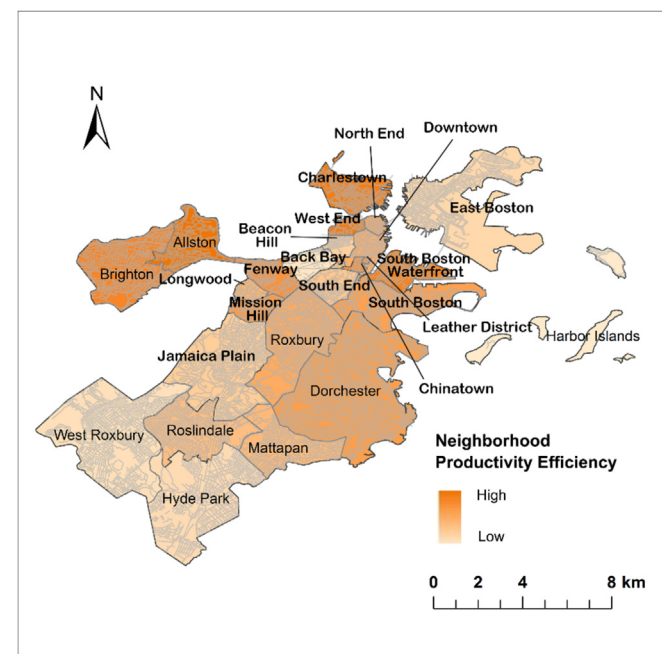


**Fig. 15.** Neighborhood productivity efficiency map of Boston.

As for the distribution, roads are more suitable for photovoltaic roads pavement in the east and northeast of Boston than the downtown and southwestern area. Further, main roads through Boston have much higher productive efficiency. Reasonably, in the downtown area, the high-rise buildings would obstruct the sky and therefore reduce the radiation. Also, the lower radiation in the southeastern rural area is inconsistent with some other studies (Li and Ratti, 2018) that attribute it to the dense tree canopy. In Fig. 10, the eastern area near the ocean shows longer insolation hours, as the coastal highways there tend to be isolated without trees and buildings surrounding them. Main roads throughout Boston receive more radiation because the wider road decreases the shade against sun from the street trees and buildings. In addition, the average traffic flow obstructing the solar panels could cut off only about 5 percent of the total street radiation without traffic, which illustrates little impact of traffic on road power generation.

The contribution and scientific significance of this research are as follows. First, we propose a complete methodological framework with wide application to measure the capacity of a city's photovoltaic road and assess the value of each solar road for better urban planning. Our expectation is to realize the wide construction of solar roads with the help of our practical computing framework. Second, we take many factors affecting radiation into account, including climate, seasons, daylight duration, buildings, trees, terrain, especially traffic to quantify radiation accurately. Third, using GSV images for calculation is more real in street simulation with low-cost compared to 3-D urban models and high-resolution satellite images. Also, GSV expands street view's application in urban construction to help decision-making.

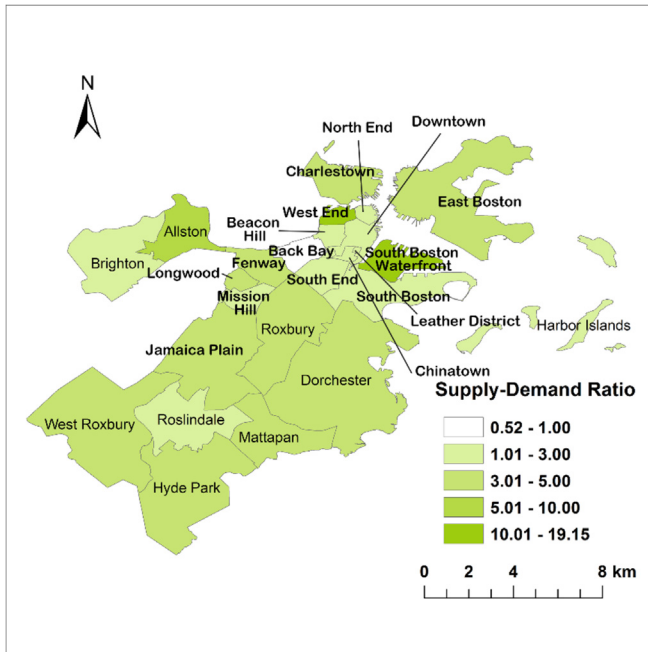


Fig. 16. The supply-demand ratio of Boston neighborhoods.

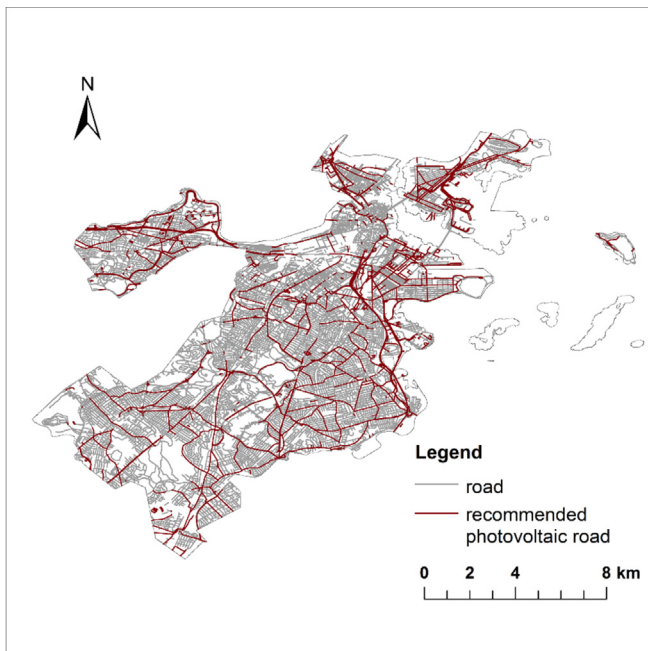


Fig. 17. Recommended PV roads in Boston.

Although results are impressive, limitations exist in this research. First, we only choose Boston for case study that may lack of representativeness and persuasiveness, because different type place's solar radiation and traffic condition have big difference, which will be improved in our future work. Second, images obtained in our study are mainly taken in summer and result in less calculated radiation in winter due to the fallen leaves of coverage. What's more, the binarization of pictures can lead to inaccuracy because blue windows may be recognized as sky incorrectly. For a more accurate estimation, it can be further developed by adopting a deep learning method to recognize the sky portion which is also

one of our future work. Besides, outside our study, the development solar road faces greater challenges like the cleaning and high cost of panels, etc.

## 6. Conclusion

In favor of the development of electric vehicles, we assume to use road surface for electricity generation. This paper proposes a novel framework of methodology to calculate the usable solar radiation in a street environment based on the street view, solar radiation model and traffic flow model. We find that all the roads in Boston can supply 763.1 thousand electric cars to travel in the downtown area annually, which shows the strong potential of road power generation. The average traffic flow obstructing the solar panels cuts off only about 5 percent street radiation, which illustrates little impact of traffic on road power generation. Neighborhoods like Allston, West End, Charlestown are more suitable for extensive photovoltaic roads laying, while in Downtown with low overall productivity efficiency, the main roads are recommended for their higher production. Since paving solar panels needs high cost, we recommend the most efficient roads for economy.

As a result, this study provides a universal scientific basis for the policy development of a Sustainable energy city, especially for the photovoltaic road construction. There is no doubt that urban road surfaces are valuable resources in generating solar power. Even more, they can support traffic energy consumption within that city without asking for more space to build solar farms and as Sahara (Yan Li, 2018) found, long distance transmission infrastructure. Particularly, many projects are under way and have made a practice (Table 1), which proves the technical feasibility of photovoltaic road. However, the construction cost still needs struggle for a long way to be reduced and demands more efficient solar road planning. In brief, these problems are not our focus.

Our study can also be applied in any other cities with street view and developed by considering the urbanization. Areas with higher urbanization level would be in larger demand of solar energy, compared with rural areas with less transportation. Usage of solar energy would be more effective if we paved solar panels in the area with large amount of radiation and high urbanization level.

## Funding

This work was supported by the National Student Innovation and Entrepreneurship Training Program of Wuhan University (No. S2018205414).

## Acknowledgement

The authors are grateful to Timothy Prestby, University of Wisconsin, Madison for his proof reading the article.

## References

- Ahmad, M.J., Tiwari, G.N., 2011. Solar radiation models—a review. *Int. J. Energy Res.* 35, 271–290.
- Ali-Toudert, F., Mayer, H., 2006. Numerical study on the effects of aspect ratio and orientation of an urban street canyon on outdoor thermal comfort in hot and dry climate. *Build. Environ.* 41 (2), 94–108.
- Alnaser, W.E., Silva, J.P., Sayigh, A.A., 2017. Solar Radiation and Street Temperature as Function of Street Orientation. An Analysis of the Status Quo and Simulation of Future Scenarios towards Sustainability in Bahrain, E3S Web of Conferences.
- Angelov, D., Dulong, C., Filip, D., Frueh, C., Lafon, S., Lyon, R., Ogale, A., Vincent, L., Weaver, J., 2010. Google street view: capturing the world at street level. *Computer* 43 (6), 32–38.
- Austin, R., 2018. How Much Do Solar Windows Cost? Are They a Viable Alternative? <https://understandingsolar.com/solar-windows-cost/>. (Accessed 12 March 2019).
- Bojanowski, J.S., Donatelli, M., Skidmore, A.K., Vrieling, A., 2013. An auto-calibration procedure for empirical solar radiation models. *Environ. Model. Softw* 49 (11),

- 118–128.
- Cao, B., Zhang, C., Bai, Z., Li, J., 2004. Technology progress and trends of electric vehicles. *J. Xi'an Jiaot. Univ.* 38 (1), 1–5.
- Carrasco-Hernandez, R., Smedley, A.R.D., Webb, A.R., 2015. Using urban canyon geometries obtained from Google Street View for atmospheric studies: potential applications in the calculation of street level total shortwave irradiances. *Energy Build.* 86 (86), 340–348.
- Cedar Lake Ventures, 2018. Weather spark. <https://weatherspark.com/y/26197/Average-Weather-in-Boston-Massachusetts-United-States-Year-Round>. (Accessed 20 May 2018).
- Chegaar, M., Chibani, A., 2000. A simple method for computing global solar radiation. *Rev. Energ. Ren. Chemss.* 111–115.
- Chen, L., Ng, E., An, X., Ren, C., Lee, M., Wang, U., He, Z., 2012. Sky view factor analysis of street canyons and its implications for daytime intra-urban air temperature differentials in high-rise, high-density urban areas of Hong Kong: a GIS-based simulation approach. *Int. J. Climatol.* 32 (1), 121–136.
- Cheng, Y., 1995. Mean shift, mode seeking, and clustering. *IEEE Trans. Pattern Anal. Mach. Intell.* 17 (8), 790–799.
- Chopra, S., Bauer, P., 2013. Driving range extension of EV with on-road contactless power transfer—a case study. *IEEE Trans. Ind. Electron.* 60 (1), 329–338.
- Chou, M.D., 1992. A solar radiation model for use in climate studies. *J. Atmos. Sci.* 49, 762–772, 1992.
- Contributor, p., 2016. Looking at the Dutch Solar Bike Path after One Year. <https://triplepundit.com/story/2016/looking-dutch-solar-bike-path-after-one-year/29346>. (Accessed 10 December 2018).
- Cooke, L., 2017. New 1 Km Solar Road Opens in Jinan, China. (Accessed 10 March 2019).
- López, Cristina S. Polo, Sala, Mariaemma, Lavinia, Ch, Tagliabue, Frontini, Francesco, Bouziri, S., 2016. Solar radiation and daylighting assessment using the sky-view factor (SVF) analysis as method to evaluate urban planning densification policies impacts. *Energy Procedia* 91, 989–996.
- D Comaniciu, P.M., 2002. Mean shift: a robust approach toward feature space analysis. *IEEE Trans. Pattern Anal. Mach. Intell.* 24 (5), 603–619.
- Dockrill, P., 2016. The World's First Solar Road Has Opened in France. <https://www.sciencealert.com/the-world-s-first-solar-road-has-opened-in-france>. (Accessed 13 March 2019).
- Flint, A.L., Childs, S.W., 1987. Calculation of solar radiation in mountainous terrain. *Agric. For. Meteorol.* 40 (3), 233–249.
- Fu, P., Rich, P., 2002. A geometric solar radiation model with applications in agriculture and forestry. *Comput. Electron. Agric.* 37 (1), 25–35.
- Gennusa, M.L., Nucara, A., Pietrafesa, M., Rizzo, G., 2007. A model for managing and evaluating solar radiation for indoor thermal comfort. *Sol. Energy* 81 (5), 594–606.
- Gilpin, L., 2014. How 'Solar Roadways' Plans to Create Smart Roads to Produce Clean Energy and Save Lives and Money. <https://www.techrepublic.com/article/how-solar-roadways-plans-to-create-smart-roads-to-produce-clean-energy-and-save-lives-and-money/>. (Accessed 10 March 2019).
- Greenshields, B.D., 1935. A study of highway capacity. In: *Proceedings Highway Research Record*, vol 14, pp. 448–477.
- Greenshields, B.D., Bibbins, J.R., Channing, W.S., Miller, H.H., 1934. A Study of Traffic Capacity. Highway Research Board Proceedings Highway Research Board, Washington, D.C.
- Hofierka, J., Kaňuk, J., 2009. Assessment of photovoltaic potential in urban areas using open-source solar radiation tools. *Renew. Energy* 34 (10), 2206–2214.
- Hong-Wu, L.I., 2006. Cellular automata model of urban road traffic flow based on characteristic of traffic density and speed. *J. Trans. Syst. Eng. Inform. Technol.* 6 (3), 71–74.
- ITRPV, I.T.R.F.P., 2018. International Technology Roadmap for Photovoltaic Results 2017. International Technology Roadmap for Photovoltaic (ITRPV), Germany.
- Jacobson, M.Z., 2009. Review of solutions to global warming, air pollution, and energy security. *Energy Environ. Sci.* 2 (2), 148–173.
- Kamat, P.V., 2007. Meeting the clean energy Demand: nanostructure architectures for solar energy conversion. *J. Phys. Chem. C* 111 (7), 2834–2860.
- Kenworthy, J.R., 2006. The eco-city: ten key transport and planning dimensions for sustainable city development. *Environ. Urbanization* 18 (1), 67–85.
- Kessels, J.T.B.A., Rosca, B., Bergveld, H.J., Bosch, P.P.J.V.D., 2011. On-line Battery Identification for Electric Driving Range Prediction, Vehicle Power and Propulsion Conference, pp. 1–6.
- Kim, Y., Keller, H., 2008. Analysis of characteristics of the dynamic flow-density relation and its application to traffic flow models. *Transport. Plann. Technol.* 31 (4), 369–397.
- Lee, K., 2016. World's First Kilometer of Solar Road Cost A Mere \$5.2 Million. <https://jalopnik.com/worlds-first-kilometer-of-solar-road-cost-a-mere-5-2-m-1790414093>. (Accessed 10 March 2019).
- Li, X., Ratti, C., 2018. Mapping the spatio-temporal distribution of solar radiation within street canyons of Boston using Google Street View panoramas and building height model. *Landsc. Urban Plann.* <https://doi.org/10.1016/j.landurbplan.2018.07.011>. (Accessed 2 August 2018) In press.
- Liang, Y., 2017. China's Solar Expressway Meets Light of Day. [http://www.xinhuanet.com/english/2017-12/28/c\\_136857894.htm](http://www.xinhuanet.com/english/2017-12/28/c_136857894.htm). (Accessed 12 March 2019).
- Lima, A., Melnik, M., Borella, N., 2011. Boston in Context: Neighborhoods 2007–2011 American Community Survey 2010 Census, pp. 1–30.
- Long, Y., Liu, L., 2017. How green are the streets? An analysis for central areas of Chinese cities using Tencent Street View. *PLoS One* 12 (2), e0171110.
- Macdonald, F., 2015. The Solar Road in The Netherlands Is Working Even Better than Expected. <https://www.sciencealert.com/solar-roads-in-the-netherlands-are-working-even-better-than-expected>. (Accessed 13 March 2019).
- MAPC, T.M.A.P.C., 2018. Data-Mapc. <https://www.mapc.org/learn/data/>. (Accessed 1 September 2018).
- Matzarakis, A., Rutz, F., Mayer, H., 2010. Modelling radiation fluxes in simple and complex environments: basics of the RayMan model. *Int. J. Biometeorol.* 54 (2), 131–139.
- Mk, S., 2010. Sky view factor analysis – implications for urban air temperature differences. *Meteorol. Appl.* 11 (3), 201–211.
- Northmore, A., 2014. Canadian Solar Road Panel Design: A Structural and Environmental Analysis. UWSpace.
- Northmore, A., Tighe, S., 2012. Innovative pavement design: are solar roads feasible?. In: *Conference of the Transportation Association of Canada*. Fredericton New Brunswick, Canada.
- Otsu, N., 1979. A threshold selection method from gray-level histograms. *IEEE Trans. Syst. Man Cybern.* 9 (1), 62–66.
- Pearcy, R.W., 1989. Radiation and light measurements. *Plant Physiol. Ecol. Field Meth. Instrum.* 97–116.
- Rahman, M.W., Mahmud, M.S., Ahmed, R., Rahman, M.S., Arif, M.Z., 2018. Solar Lanes and Floating Solar PV: New Possibilities for Source of Energy Generation in Bangladesh. *Power & Advanced Computing Technologies*.
- Rich, P.F.a.P.M., 2000. In: Institute(HEMI), H.E.M. (Ed.), *The Solar Analyst 1.0 User Manual* (USA).
- Rich, P.M., 1989. A Manual for Analysis of Hemispherical Canopy Photography. United States.
- Rich, P.M., 1990. Characterizing plant canopies with hemispherical photographs. *Rem. Sens. Environ.* 5 (1), 13–29.
- Roadways, S., 2018. Welcome to Solar Roadways. <http://www.solarroadways.com/Home/Index>. (Accessed 10 March 2019).
- Rooij, R.v., 2017. Dutch Solar Bike Path SolarRoad Successful & Expanding. <https://cleantechica.com/2017/03/12/dutch-solar-bike-path-solaroad-successful-expanding/>. (Accessed 10 March 2019).
- Rousselet, J., Imbert, C.E., Dekri, A., Garcia, J., Goussard, F., Vincent, B., Denux, O., Robinet, C., Dorkeld, F., Roques, A., 2013. Assessing species distribution using Google street view: a pilot study with the pine processionary moth. *PLoS One* 8 (10), e74918.
- Rundle, A.G., Bader, M.D.M., Richards, C.A., Neckerman, K.M., Teitler, J.O., 2011. Using Google street view to audit neighborhood environments. *Am. J. Prev. Med.* 40 (1), 94–100.
- Sirmacek, B., 2011. Graph Theory and Mean Shift Segmentation Based Classification of Building Facades. *Urban Remote Sensing Event*.
- Súri, M., Hofierka, J., 2010. A new GIS-based solar radiation model and its application to photovoltaic assessments. *Trans. GIS* 8 (2), 175–190.
- Swift, L.W., 1976. Algorithm for solar radiation on mountain slopes. *Water Resour. Res.* 12 (12), 108–112.
- Torii, A., Havlena, M., Pajdla, T., 2009. From Google street view to 3D city models. In: *IEEE International Conference on Computer Vision Workshops*, pp. 2188–2195.
- U. S. Environmental Protection Agency, U.S. Department of Energy, 2018. 2018 Tesla Model (All Models). *Fueleconomy.Gov*. (Accessed 10 December 2018).
- Unger, J., 2009. Connection between urban heat island and sky view factor approximated by a software tool on a 3D urban database. *Int. J. Environ. Pollut.* 36 (1/2/3), 59.
- Watson, I.D., Johnson, G.T., 2010. Graphical estimation of sky view-factors in urban environments. *Int. J. Climatol.* 7 (2), 193–197.
- Ya'u, M.J., Gele, M.A., Ali, Y.Y., Alhaji, A.M.i., 2018. Global solar radiation models: a review. *J. Photonic Mater. Technol.* 4 (1), 26–32.
- Yan Li, E.K., Safa, Motesharrei, Jorge, Rivas, Fred, Kucharski, Kirk-Davidoff, Daniel, Bach, Eviatar, Zeng, Ning, 2018. Climate model shows large-scale wind and solar farms in the Sahara increase rain and vegetation. *Science* 3261 (6406), 1019–1022.
- Zamir, A.R., Darino, A., Shah, M., 2012. Street View Challenge: Identification of Commercial Entities in Street View Imagery, *International Conference on Machine Learning and Applications and Workshops*, pp. 380–383.
- Zhang, F., Zhou, B., Liu, L., Liu, Y., H., F.H., et al., 2018. Measuring human perceptions of a large-scale urban region using machine learning. *Landsc. Urban Plann.* 180, 148–160.
- Zhao, F.W., Zhao, B.J., 2015. Research on the development strategies of new energy automotive industry based on car charging stations. *Appl. Mech. Mater.* 740, 985–988.